

# Near-Infrared Lab-on-a-Chip Optical Biosensor with Micro Ring Resonator and Fourier Transform Spectrometer on SOI platform

Kyoung Min Yoo<sup>1,2</sup>, Kang-Chieh Fan<sup>2</sup>, Yue An<sup>2</sup>, May Hlaing<sup>3</sup>, Sourabh Jain<sup>2</sup>, and Ray T. Chen<sup>2,3</sup>

<sup>1</sup>Synopsys Inc., 1301 South Mopac Exp., Bldg. 4, Suite 200, Austin, TX, 78746, USA.

<sup>2</sup>Department of Electrical and Computer Engineering, The University of Texas at Austin, 10100 Burnet Rd. Austin, TX, 78758, USA.

<sup>3</sup>Omega Optics Inc., 8500 Shoal Creek Blvd., Bldg. 4, Suite 200, Austin, TX, 78757, USA.

Author e-mail address: [yook@synopsys.com](mailto:yook@synopsys.com), [chenrt@austin.utexas.edu](mailto:chenrt@austin.utexas.edu)

**Abstract:** We demonstrated the design and experimental results of the near-infrared lab-on-a-chip optical biosensor platform that monolithically integrates the micro-ring-resonator and the on-chip spectrometer on the SOI wafer with the limit of detection of 0.042 RIU. © 2023 The Author(s)

As the needs of the accurate and fast point-of-care portable bio-detection systems are growing rapidly for the clinical and health-monitoring applications, a micro-ring-resonator (MRR) optical biosensor based on the evanescent field sensing mechanism has been extensively studied due to its high sensitivity and compact device size [1,2]. Generally, the bulk sensing sensitivity ( $S$ ) of the MRR biosensor is defined as  $S = \frac{\Delta\lambda}{\Delta n_{\text{clad}}}$ ... (1) where  $\Delta\lambda$  is the resonance wavelength shift, and  $\Delta n_{\text{clad}}$  is the change of the cladding refractive index. Also, the limit-of-detection (LOD) of the sensor depends on the minimum resolvable wavelength shift, which is determined by the measurement setup [2]:  $\text{LOD} = (\Delta\lambda_{\text{min}})/S$ ... (2). Here,  $\Delta\lambda_{\text{min}}$  is the minimum detectable resonance wavelength shift, which is the optical spectrum analyzer's measurement resolution ( $\delta\lambda$ ). Several research have presented high- $S$  MRR bio-sensing applications in near-infrared wavelength with advanced structures including sub-wavelength grating (SWG) based waveguides [3], and cascaded resonators utilizing Vernier effects to maximize the sensing sensitivity; but utilizing external optical spectrum analyzer (OSA) was inevitable to read the spectrum and detect  $\Delta\lambda$  in any case, which makes the overall system bulky and expensive. For the miniaturized lab-on-a-chip applications, a suitable on-chip integrated spectrometer device has to be demonstrated which can read  $\Delta\lambda$  from MRR biosensors based on minuscule changes in refractive index. In this paper, we demonstrated the design and experimental results of the near-infrared lab-on-a-chip optical biosensor platform that monolithically integrates the MRR and the on-chip spectrometer on the silicon-on-insulator (SOI) wafer, which can eliminate the external optical spectrum analyzer for scanning the wavelength spectrum. The basic device configuration and working principle are demonstrated in Fig. 1.

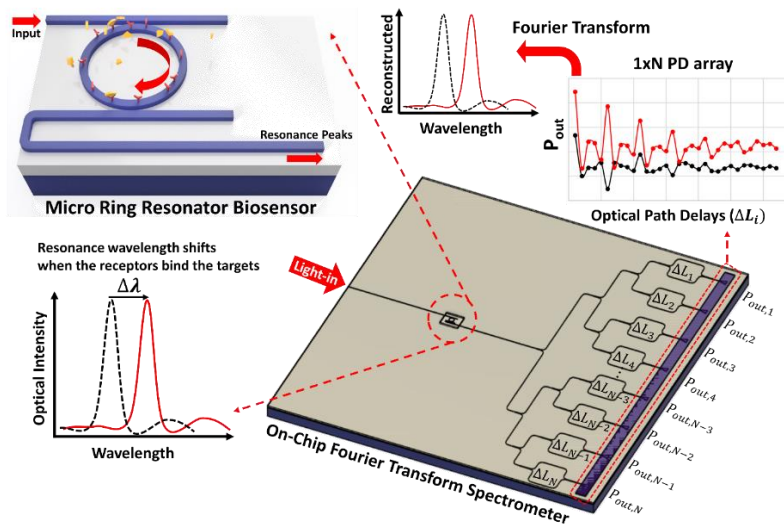


Fig. 1. Schematic illustration of the operation principle of the on-chip spectrometer integrated optical biosensor platform; PD: photodetector

The MRR is a biosensing device which configures the resonance peaks from the drop-port output, and the evanescent field is altered when the molecular binding takes place between the immobilized bioreceptors and target

analytes in the sample which changes the resonance condition leading to a resonance wavelength shift ( $\Delta\lambda$ ). The drop-port of MRR is directly connected to the spatial heterodyne Fourier transform Spectrometer (SHFTS), that is composed of an array of unbalanced MZIs with linearly increasing optical path delays ( $\Delta L_i$ ). The phase change from each MZI is converted into an intensity change based on interferometric schemes, constituting the interferogram of the output powers ( $P_{out, N}$ ) [4]. Output powers from each MZIs can be measured by the integrated photodetector (PD) array [5], and the input spectrum from the MRR drop-port is reconstructed through the discrete Fourier transform equation (DFT):  $p^{in}(\bar{\sigma}) = \frac{\Delta x}{N} p^{in} + 2 \frac{\Delta x}{N} \sum_{i=1}^N F(x_i) \cos 2\pi \bar{\sigma} x_i$ , where  $F(x_i) = \frac{1}{B_s} (2P_i^{out} - A_s P^{in}) \dots (3)$ . Here,  $\sigma$  is the wavenumber, and  $\bar{\sigma} = \sigma - \sigma_{min}$  is the shifted wavenumber, where  $\sigma_{min}$  represents the minimum wavenumber.  $x_i = n_{eff} \Delta L_i$ , where  $n_{eff}$  is the effective index of the strip waveguide and  $\Delta x$  is the maximum delay, and  $A_s$  and  $B_s$  are the coupling and loss coefficients of the MZI components [4]. The MRR and SHFTS are designed for the center operation wavelength of 1550 nm, and the layer thicknesses of the SOI wafer and the strip waveguide are designed for guiding the fundamental transverse-electric (TE) mode; the width and thickness of the silicon strip waveguide are 500 nm and 220 nm. Based on the single TE mode, we designed and fabricated the MRR and SHFTS devices and experimentally tested the device performances. The overall layout of the integrated circuit is shown in Fig. 2(a).

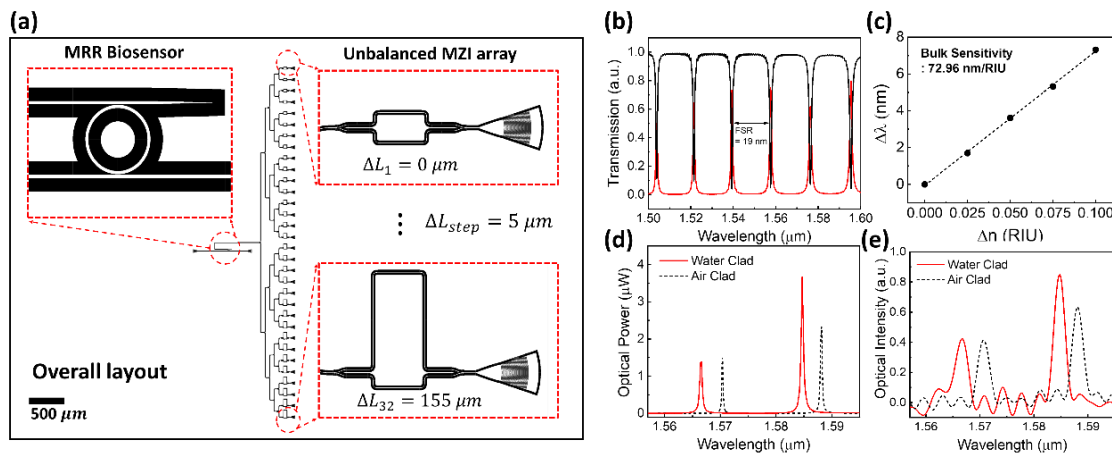


Fig. 2. MRR-SHFTS integrated biosensor design and measurement results. (a) Overall layout of the integrated biosensor. (b) MRR transmission spectrum from the through port and drop port; black-line: through port, red-line: drop port. (c) MRR resonance wavelength shift based on the refractive index change of the top-cladding. (d) MRR drop-port measurement results using external OSA. (e) MRR drop-port spectrum reconstructed from SHFTS; black-line: air top cladding, red-line: water top cladding.

The MRR design parameters include the gap-distance ( $d$ ) between the bus- and ring-waveguide to ensure the critical coupling based on the couple mode theory [1], and the diameter of the ring resonator ( $D$ ) is designed to get the large enough FSR to make it compatible with the SHFTS spectral resolution and bandwidth. The device parameters are optimized by the 3D FDTD simulation, as  $d=70$  nm and  $D=10$   $\mu\text{m}$ , and the optical characteristics are measured as  $\text{FSR}=19$  nm, and  $Q=4000$  from optimized structure (Fig. 2(b)). Then, the refractive index of the top cladding is changed ( $\Delta n_{clad}$ ) and the resonance wavelength shift ( $\Delta\lambda$ ) is measured to calculate the bulk-sensing sensitivity of the biosensor that is presented in Fig. 2(c). The bulk-sensing sensitivity is calculated as  $S=72.96$  nm/RIU. Then, the silicon SHFTS is designed to have 32-MZIs ( $N=32$ ) with the maximum path length delay ( $\Delta L$ ) of 155  $\mu\text{m}$ , which gives us the spectral bandwidth of 50 nm, and the resolution of  $\delta\lambda=3.1$  nm based on the Nyquist-Shannon sampling theory [6]. Subsequently, the limit of detection of the MRR-SHFTS integrated sensor is calculated as  $\text{LOD}=0.042$  RIU by (eq. 2). Finally, we experimentally measured the output powers of the MZI array and reconstructed the spectrum and measured  $\Delta\lambda$  by changing the MRR top claddings. Fig. 2(d) shows the MRR drop-port spectrum measurement results by OSA with different claddings, and Fig. 2(e) shows the SHFTS-MRR reconstructed spectrum. As the FTS reconstructed spectrum shows well-matching results with the direct OSA measurement results, we validated that the MRR-SHFTS integrated device can successfully substitute the external OSA for the lab-on-a-chip biosensor applications. Our proof-of-concept experiment paves the way for a monolithically integrated lab-on-a-chip optical biosensor, and we expect to improve the LOD by applying SWG-MRR sensors that we previously reported with  $S=545$  nm/RIU [3], that gives  $\text{LOD}=0.0057$  RIU. This research was supported by NSF Award #1932753.

## References

- [1] W. Bogaerts, et al., Laser & Photon. Rev., 6: 47-73 (2012)
- [2] P. Steglich, et al., Molecules 24(3), 519 (2019)
- [3] C.-W. Chang, et al., Biosens. Bioelectron. 141, 111396 (2019)
- [4] M. Florjańczyk, et al., Opt. Express 15, 18176-18189 (2007)
- [5] H. Li, et al., Nanomaterials 10 (9), 1683 (2020).
- [6] K. M. Yoo et al., ACS photonics 9(8), pp. 2691-2701 (2022).